

# Elevated Electron Temperatures in the Auroral *E* Layer Measured With the Chatanika Radar

VINCENT B. WICKWAR<sup>1</sup> AND CHANTAL LATHUILLERE<sup>2</sup>

*Radio Physics Laboratory, SRI International, Menlo Park, California 94025*

WLODEK KOFMAN AND GERARD LEJEUNE

*Centre d'Etude des Phénomènes Aléatoires et Géophysiques, BP 46, 38402 St. Martin d'Hères, France*

An extensive series of spectral measurements has been made in the auroral *E* region with the Chatanika incoherent scatter radar. Because of the small scale length for variations of electron density, temperatures, and ion-neutral collisions we used the operating mode with the best possible range resolution—9 km. About 5% of the time the data exhibited an unusual spectral shape that was most pronounced at 105 and 110 km. Instead of being almost Gaussian with only a small hint of two peaks, the spectra are much wider, with two well-developed peaks. After carefully considering the validity of the measurements and their interpretation, we conclude that the unusual spectra are due to greatly enhanced electron temperatures. At 110 km, the electron temperature may increase from 250 K to 800 K, while the ion temperature remains near 250 K. This enhancement of the electron temperature extends from 99 km to at least 116 km. We show that the temperature increase is too large to be accounted for by auroral particle precipitation, though it coincides in time with ion temperature enhancements at altitudes above 125 km. Because these latter enhancements are believed to be due to joule heating, we deduce that electric fields of 24–40 mV/m are present and that the electrons are moving through the ions and neutrals at speeds of 500–800 m/s. Despite these velocities, we find that joule heating of the electrons also cannot account for the elevated electron temperatures. Several consequences of the elevated electron temperatures are discussed. One is that the rate constants for molecular recombination are reduced. Another is that during periods of significant joule heating, the deduced electron density profile, when fully corrected for temperatures, has a significantly lower peak altitude and greater density than that deduced under the usual assumption of equal electron and ion temperatures. Since conductivities, currents, ionization rates, and differential energy spectra are dependent upon the density profile, care must be taken to account properly for the temperature effects when deriving these quantities.

## INTRODUCTION

The interpretation of a large portion of the data acquired with the Chatanika incoherent scatter radar has involved the use of the electron density that comes from the total power in the return signal and the ion velocity that comes from the Doppler shift of the return signal. In this paper we examine the details of the shape of the power spectrum of this returned signal. The spectral shape is the result of the combined effects of electron and ion temperatures, ion mass, and ion-neutral collisions [e.g., *Evans*, 1969]. Because the temperatures and the neutral densities are changing rapidly with altitude in the auroral *E* layer, the data have to be acquired with as good an altitude resolution as possible. A large body of such spectral data was acquired with the multipulse autocorrelator (MAC) [*Rino et al.*, 1974] with a 9-km altitude resolution during the joint American-French plasma line experiments in 1978 [*Kofman and Wickwar*, 1980].

Here we report on an unusual feature of the incoherent scatter spectrum that we observed between 99 and 116 km in a small portion of the data. These unusual spectra are due to greatly increased electron temperatures. This finding was quite unexpected according to a large body of theoretical work [e.g., *Rees and Walker*, 1968; *Walker and Rees*, 1968;

*Rees et al.*, 1971]. We, too, cannot account for these elevated electron temperatures by either particle precipitation or joule heating. Nonetheless, the electron temperature enhancements occur simultaneously with strong joule heating of the ions at higher altitudes. Because of the unexpected nature of these temperatures, we have made a considerable effort to ensure that the measurements are good and that the temperature interpretation is correct.

In the next section, we describe the measurements. Then we present the analysis that leads us to believe that these observations are of elevated electron temperatures. We further describe the phenomenon and the conditions under which it occurs. In the final section we discuss these findings and their implications and give our conclusions.

## OBSERVATIONS

The observations were made at Chatanika, Alaska, with the incoherent scatter radar [*Leadabrand et al.*, 1972] pointing along the magnetic field line. *E* region spectral measurements were made simultaneously with *F* region spectral measurements and plasma line measurements [*Kofman and Wickwar*, 1980]. The *E* region measurements themselves were obtained with a variant of the multipulse technique described by *Rino et al.* [1974]. In this technique a single 60- $\mu$ s pulse is transmitted, followed one interpulse period later by a burst of three 60- $\mu$ s pulses that begin at 0, 100, and 340  $\mu$ s. Samples of the IF acquired at 10- $\mu$ s intervals from the first pulse and the multipulse burst enable a 320- $\mu$ s autocorrelation function (ACF) to be obtained containing alternate samples of the real and imaginary parts.

<sup>1</sup>Present address is Division of Atmospheric Sciences, National Science Foundation, Washington, D. C. 20550.

<sup>2</sup>Permanent address is Centre d'Etude des Phénomènes Aléatoires et Géophysiques, BP 46, 38402 St. Martin d'Hères, France.

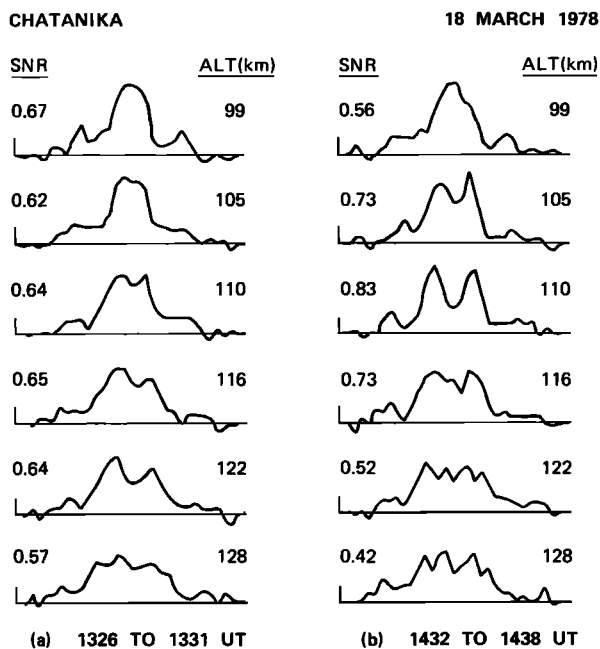


Fig. 1. E region spectra from March 18, 1978, obtained with the multipulse autocorrelator using a 60- $\mu$ s unipulse followed one interpulse period later by a burst of three 60- $\mu$ s pulses that started at 0, 100, and 340  $\mu$ s. The spectral window is 50 kHz wide. The two time periods were selected, in part, because of similar signal-to-noise ratios. (a) Typical spectra measured between 1326 and 1331 UT. (b) Unusual spectra measured between 1432 and 1438 UT. In particular, they are unusual at 105 and 110 km, though at 116 km the spectrum is still considerably wider than that in the earlier time period.

In presenting the observations, we can consider either the ACF or its equivalent Fourier transform, the power spectrum. As an aid to discussion, we present the spectra. In Figure 1a, we show typical spectra from a medium-sized auroral layer (i.e., peak density of  $2 \times 10^5 \text{ cm}^{-3}$ ) from 99 to 128 km. They were obtained between 1326 and 1331 UT on March 18, 1978. (Note that 1130 UT is 0130 Alaska Standard Time and is approximately magnetic midnight.) At the two lowest altitudes, the spectra are almost Gaussian. At the next three higher altitudes, they increasingly take on a two-humped shape characteristic of most incoherent scatter spectra. (The bumps in the wings are an artifact of the multipulse technique [Rino *et al.*, 1974].)

In Figure 1b we show a similar series of spectra obtained an hour later, between 1432 and 1438 UT on March 18, 1978. They are typical of the unusual spectra that we found. At the four lowest altitudes the spectra are considerably wider than those shown in Figure 1a. Much more dramatic, however, is the two-humped nature of the spectra at 105 and 110 km and the very pronounced valley in the center of the spectrum at 110 km. By 128 km the spectra in Figures 1a and 1b are very similar.

#### ANALYSIS AND INTERPRETATION

The unknown ionospheric parameters of interest are determined from the measured data by using the ACFIT program [Lejeune, 1978, 1979; de la Beaujardiere *et al.*, 1980]. This program performs a nonlinear least squares fit of calculated ACF's to the observed ACF. The procedure is iterative, each calculated ACF being the Fourier transform of the incoherent scatter spectrum calculated for a set of fixed and a set of un-

known ionospheric parameters. The unknown variables are incremented after each fit until a convergence criterion is achieved. This procedure produces the best estimate of the unknown ionospheric parameters and their uncertainties. The iterative procedure is a modified steepest descent method [Bevington, 1969; Hagfors, 1978].

Because some aspects of the analysis of the multipulse data in this mode are different from the analyses described in the literature, we show some of the pertinent steps in the appendix.

The theory incorporated into the program for the calculation of the incoherent scatter spectra includes most known

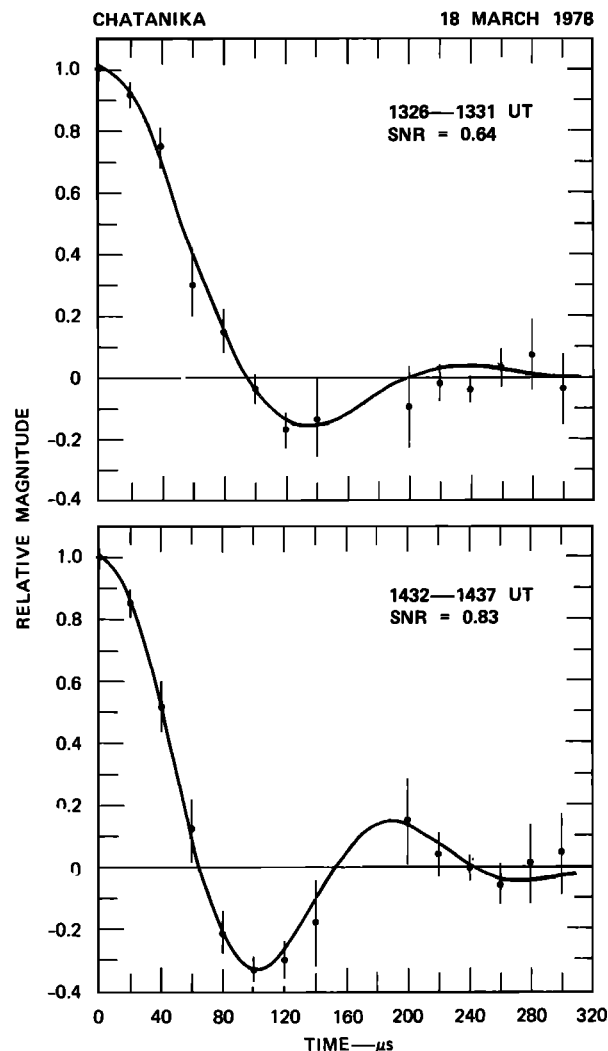


Fig. 2. Fitted and measured normalized autocorrelation functions for 110 km on March 18, 1978. The lines show the real part of the calculated best fit ACF's,  $\text{Re } \rho_{\text{TH}}(t)$ , from (A6). The solid circles show the real part of the observed ACF's fully corrected for the complex weighting function,  $\text{Re } R_{\text{OBS}}(t)e^{-i\omega t}$ , from (A4) and (A5). The error bars are calculated according to (A8a)–(A8c) and are scaled by  $[S(t)S^*(t)]^{-1}$ . The points at 160 and 180  $\mu$ s have exceedingly large uncertainties because the magnitude of  $S(t)$  is nearly zero. Consequently, they have been omitted. (a) Observed and fitted ACF's for the typical period 1326–1331 UT. The values of  $N_e$ ,  $T_e$ ,  $T_b$ , and  $\nu_{in}$  are  $2.0 \pm 0.3 \times 10^5 \text{ cm}^{-3}$ ,  $270 \pm 30 \text{ K}$ ,  $280 \pm 70 \text{ K}$ , and  $1300 \text{ s}^{-1}$  and the fit parameter  $\sqrt{\chi_R^2}$  (A7) is 0.72. (b) Observed and fitted ACF's for the unusual spectrum observed in the period 1432–1438 UT. The values of  $N_e$ ,  $T_e$ ,  $T_b$ ,  $\nu_{in}$ , and  $\sqrt{\chi_R^2}$  are  $2.7 \pm 0.3 \times 10^5 \text{ cm}^{-3}$ ,  $670 \pm 50 \text{ K}$ ,  $280 \pm 30 \text{ K}$ ,  $1300 \text{ s}^{-1}$ , and 0.50, respectively. The major difference is the elevated  $T_e$ .

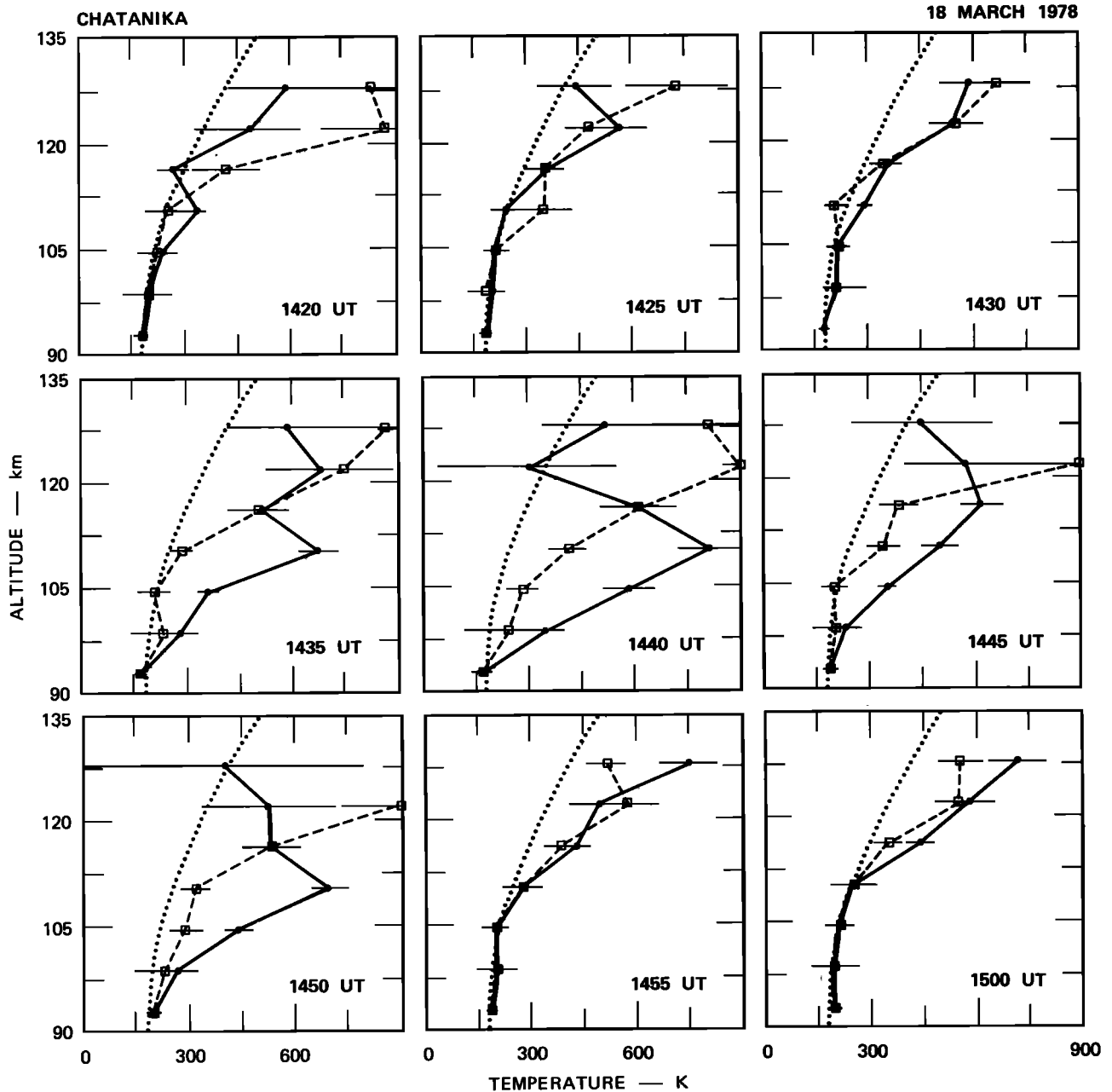


Fig. 3. Sequence of *E* region temperature profiles for March 18, 1978. The dotted curve in each is the temperature profile from the *Jacchia* [1971] model for a 1000 K exospheric temperature. It is an indication of the neutral temperature, but above all it is a convenient reference. The points connected by solid line segments are the electron temperatures. The points connected by dashed line segments are the ion temperatures.

plasma effects that would affect the shape of the spectrum. As a consequence, with ACFIT it is possible, in principle, to determine as many as ten parameters; however, the data are never precise enough to do so. Indeed, the challenge in applying ACFIT is to reduce the number of unknown parameters enough so that the uncertainties in the results are small, while simultaneously retaining enough parameters to adequately describe the physical situation. The most important parameters in the auroral *E* region are the ion velocity, the electron density, the electron and ion temperatures, and the ion-neutral collision frequency. While the ion velocity has little impact on deriving the other parameters, the effects on the spectrum of the last three parameters are strongly coupled. In

order to find these parameters, we have had to perform a series of fits so as to determine some of the parameters sequentially rather than simultaneously.

Our procedure has taken advantage of the fact that the ion-neutral collision frequency  $\nu_m$  is the most stable variable. Its mean profile was found from seven nights in March 1978 by selecting periods when we could assume that the electron and ion temperatures were equal between 93 and 116 km—i.e., periods when there was no joule heating and little precipitation. The resultant profile is similar to that obtained from the *Jacchia* [1971] model of the neutral atmosphere, for a 1000 K exospheric temperature, and with the collision frequencies for momentum transfer in the rest frame of the ions [*Schunk and*

Walker, 1973]. Given these  $\nu_m$ , we were then able to refit the data, this time allowing the electron temperatures  $T_e$  to differ from the ion temperatures  $T_i$ .

In Figure 2a we show the quality of the fit for the "typical" data corresponding to the spectrum in Figure 1a for 110 km. The solid circles and error bars are derived from the real part of the measured ACF, and the solid line represents the theoretical ACF (see appendix). In Figure 2b we show the fit to the unusual data corresponding to the spectrum in Figure 1b for 110 km. The quality of the fit is just as good as it is for the "typical" data. However, to obtain the fit to the unusual spectrum, a much higher  $T_e$  is required: 675 K for Figure 2b versus 260 K for Figure 2a. There is very little change in  $T_i$ .

Thus a straightforward fit to the data yields an elevated electron temperature. Because such increases are unexpected, an important question is whether this interpretation is unique. We have calculated many theoretical spectra and have experimented with the fits to examine this question. The initial values of  $T_e$  and  $T_i$  used for the first iteration have no effect on the results for most of the fits. Also, at the altitude of the greatest temperature effect (110 km), and because the radar frequency is high (1290 MHz), the ion-neutral collision frequency has very little effect on the deduced electron temperature. A 25% variation in  $\nu_m$ , which is large compared to what has been seen at lower latitudes, has less than a 3% effect on  $T_e$ . If the ion and electron temperatures are forced to be more equal,  $\nu_m$  is reduced by an unacceptable amount. Indeed, if they are kept equal, the ACFIT program attempts to make the  $\nu_m$  negative (which is how we found the phenomenon). If there were meteoric ions present, for example,  $Mg^+$  and  $Fe^+$ , the spectrum would be narrower and the ACF wider, with the effect that the deduced electron temperature, which assumes a 30.5-amu ion, would be decreased instead of increased. An ion with considerably less mass would be required to deduce an elevated electron temperature, but then the ion temperature would be reduced to unacceptable values because the deduced temperature ratio is not a strong function of ion mass. Thus for the known dependence of the incoherent scatter spectrum upon the variables tested, we conclude that  $T_e$  is much greater than  $T_i$ .

By examining the analyzed data we can learn more about the reasonableness of the deduced electron temperatures and the possible presence of spurious artifacts that would affect the analysis. In Figure 3 we present the electron and ion temperature profiles around and during an isolated electron heating event on March 18, 1978, as well as the *Jacchia* [1971] temperature profile for a 1000 K exospheric temperature. In Figure 4 we present similar data from a selected period on November 19, 1978, encompassing another electron heating event. During this second period the temporal behavior is more complex. (We believe that the decrease in  $T_e$  and  $T_i$  in going from 93 to 99 km in November is due to our use of a  $\nu_m$  profile optimized for March.) On both days we have periods of minimum  $T_e$  (and  $T_i$ ): 1425, 1430, 1455, and 1500 UT in March and 1305, 1308, 1337, and 1342 UT in November. The other profiles show the phenomenon of interest, the elevated  $T_e$  in the vicinity of 105 and 110 km. There are particularly large enhancements at 1440 and 1450 UT in March and at 1217, 1237, and 1327 UT in November. The ion temperatures, as mentioned previously, appear practically unchanged at these altitudes when the large  $T_e$  are found. This behavior supports the idea that the fitting procedure has correctly identified  $T_e$  as the cause for the unusual spectra and ACF's.

The largest  $T_e$  increases are always at 110 km, although substantial increases often occur at 105 km. In most of the largest events listed above, there is an indication of elevated  $T_e$  at both 99 and 116 km. Unfortunately, the measurements at 99 km are not individually precise enough to ensure that  $T_e$  is elevated, but collectively they do suggest that there is an enhancement. The situation at 116 km is complicated, because  $T_e$  enhancements can occur at 116 km and higher due to the loss of energy from auroral primaries and secondaries [Rees and Walker, 1968]. However, a comparison of the data at 1237 and 1305 UT in November shows that another heat source in addition to energetic and secondary electrons is needed to account for  $T_e$  at 1237 UT. While there is more energetic electron precipitation depositing energy at 116 km at 1305 UT than at 1237 UT, the electron temperature is higher at 1237 UT.

If we go low enough in altitude, to 93 km, we find very little variation in the electron temperature. This is particularly true for the data from March, which have a more appropriate  $\nu_m$  model and a better signal-to-noise ratio (SNR). The constancy of the spectra (and ACF's) at this altitude provides a good indication that the whole radar system is working properly throughout the observing period. While this is perhaps the best such measure, another one is that our goodness of fit parameter,  $\sqrt{\chi_R^2}$  (see appendix), stays at its unusual value, close to 1, on both sides and during the elevated  $T_e$  events.

When we go up in altitude, above the region of  $T_e$  increase, we see other differences in the behavior of the temperature profiles during the period of the  $T_e$  increase. The major effect is that the ion temperature increases greatly at 122 and 128 km (to the point that it is greater than the arbitrary 900 K temperature maximum used in Figures 3 and 4). It may even increase at 116 km. There also appears to be a reduction in the electron temperature. These effects can be better examined by reference to Figures 5 and 6 for March 18, 1978, and November 19, 1978, respectively. The bottom curve in these figures shows the temporal variation of  $T_e$  at 110 km. The middle curve shows the temporal variation of  $T_i$  at 163 km. The top two curves show the variation of the electron density at 110 km and at either 99 km or 105 km. The most striking feature of these figures is the correlation between the  $T_e$  at 110 km and the  $T_i$  at higher altitude.

In a brief aside, we need to mention that the ion temperatures at 163 km were found using another correlator and a single long pulse, 320  $\mu s$ . The ion composition was assumed to be 29%  $O^+$  and 71% of our fictitious molecular ion of mass 30.5. This composition is reasonable under many conditions but most likely underestimates the proportion of molecular ions during joule heating events [Kelly and Wickwar, 1981]. Regardless of the exact ion composition, there is a strong correlation between  $T_e$  and  $T_i$ . The choice of 163 km was somewhat arbitrary. The temporal variation at 213 km is practically identical. At higher altitudes the same structures remain, but there are other underlying trends in the data.

From other work where temperatures could be determined simultaneously with ion velocities perpendicular to the magnetic field [Wickwar, 1975; de la Beaujardiere et al., 1981; Kelly and Wickwar, 1981], we know that the elevated ion temperatures are the result of joule heating. Therefore, this comparison tells us that the elevated electron temperatures near 110 km occur during particular ionospheric conditions, namely, joule heating situations.

We can estimate the ion velocity and the electric field from

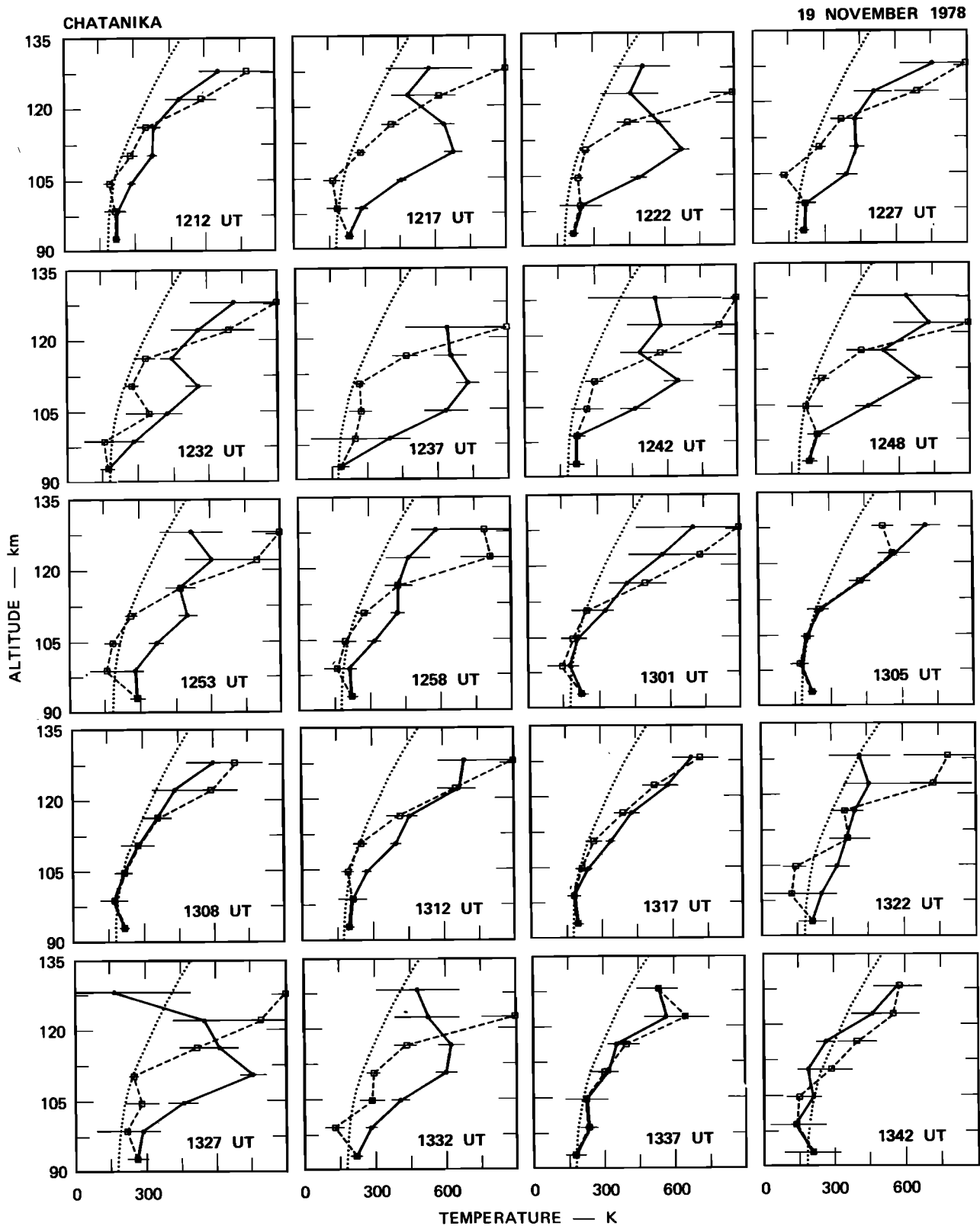


Fig. 4. Sequence of *E* region temperature profiles for November 19, 1978. The dotted curve in each is the temperature profile from the *Jacchia* [1971] model for a 1000 K exospheric temperature. It is an indication of the neutral temperature, but above all it is a convenient reference. The points connected by solid line segments are the electron temperatures. The points connected by dashed line segments are the ion temperatures.

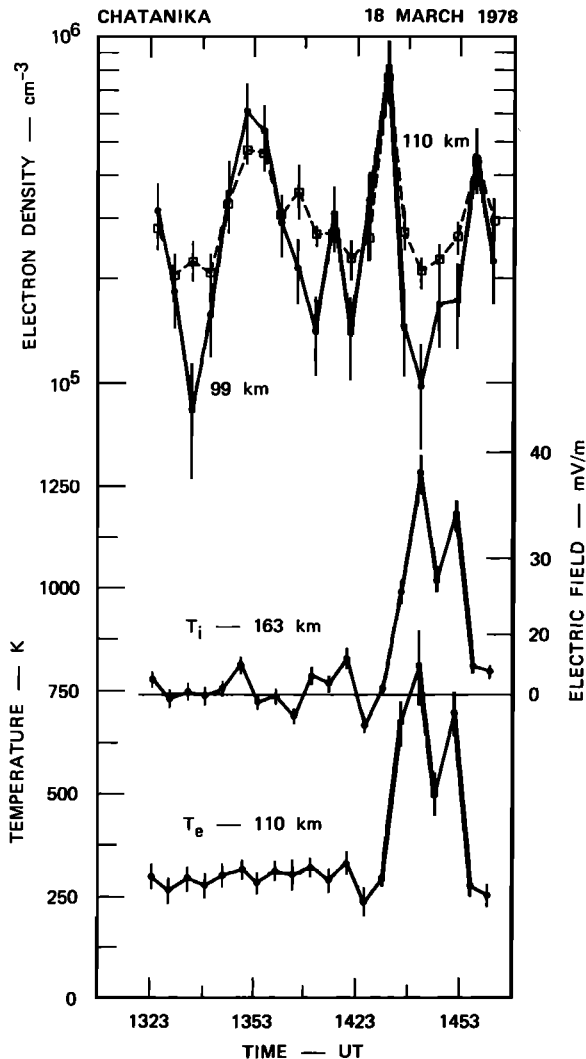


Fig. 5. Time variation of electron and ion temperatures and electron density on March 18, 1978. The bottom two curves show the covariation of  $T_e$  at 110 km and  $T_i$  at higher altitudes. The electric field scale is based on joule heating of the ions with stationary neutrals. The top two curves show the electron density variation at 99 and 110 km.

the ion temperature increase. Under steady state conditions and when heating by electrons can be omitted (as it can at 163 km), the difference between the ion and neutral temperatures for joule heating is given by [Schunk, 1975]

$$T_i - T_n = c_i(v - u)^2 \quad (1)$$

where  $v$  is the ion velocity,  $u$  is the neutral velocity, and  $c_i$  for each ion depends on the relative distribution of neutral constituents. At 163 (for the data in Figures 5 and 6),  $c_i$  is approximately  $8.5 \times 10^{-4} \text{ K s}^2/\text{m}^2$  for  $\text{O}^+$  and  $9.3 \times 10^{-4} \text{ K s}^2/\text{m}^2$  for  $\text{NO}^+$  and  $\text{O}_2^+$ . For our purposes we can neglect the differential ion heating and use a value of  $9 \times 10^{-4} \text{ K s}^2/\text{m}^2$ . We will further assume that the neutrals are stationary. Then

$$T_i - T_n \approx 9 \times 10^{-4} v^2 \quad (2)$$

enables us to estimate the ion velocity. Furthermore, above about 150 km the ion equation of motion is

$$v = -E \times B \quad (3)$$

enabling us to estimate the electric field. Assuming that the field lines are equipotentials and noting that (3) is also the electron equation of motion above about 80 km, then (2) applied to ions near 165 km also gives a good estimate of the electron velocity above 85 km.

In Figures 5 and 6 we have drawn lines near the lowest ion temperatures to indicate the estimated  $T_n$ . We have then marked an electric field along the right axis according to (2) and (3). The velocities in meters per second are numerically 20 times the electric field in millivolts per meter. There are clear cases of elevated electron temperatures for electric fields of 25–40 mV/m or electron velocities of 500–800 m/s. These are large electric fields and velocities.

It would be practically impossible to find a problem in the radar system or in the analysis that could at the same time cause a  $T_e$  increase in one altitude region and a  $T_i$  increase in another. Thus the fact that we can correlate the occurrence of this low-altitude electron heating to another physical phenom-

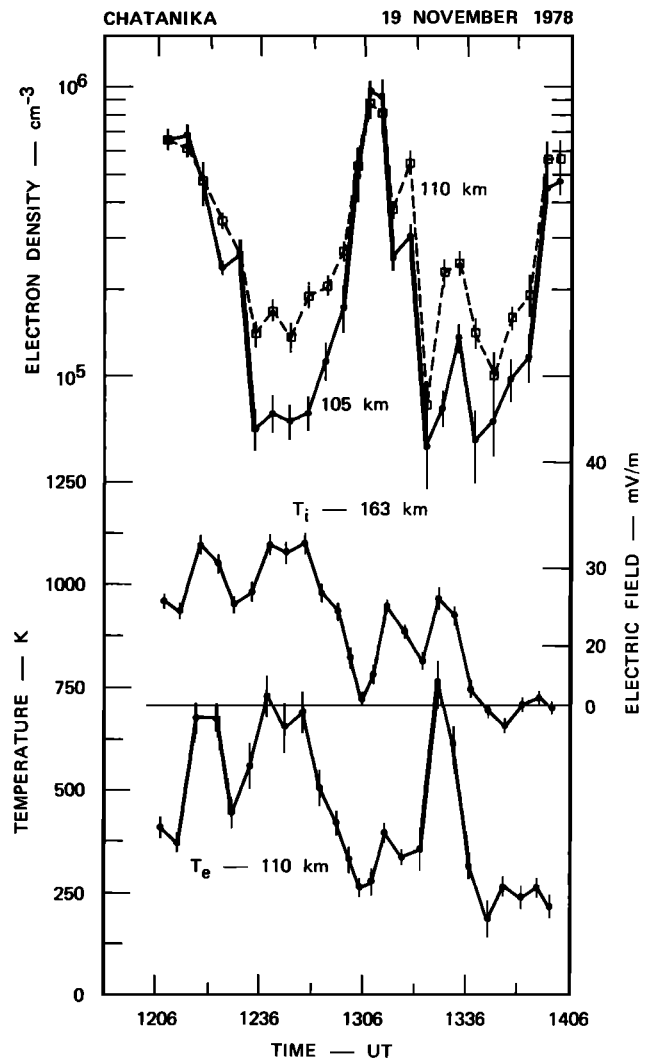


Fig. 6. Time variation of electron and ion temperatures and electron density on November 19, 1978. The bottom two curves show the covariation of  $T_e$  at 110 km and  $T_i$  at higher altitudes. The electric field scale is based on joule heating of the ions with stationary neutrals. The top two curves show the electron density variation at 105 and 110 km.

enon, the occurrence of joule heating, should remove any lingering doubt about the reality of the  $T_e$  measurements.

The electron density curves, one at 110 km and one at a lower altitude where there is still substantial ionization, show no correlation with the elevated electron temperatures near 110 km. Between 1323 and 1425 UT in March there is practically no variation in  $T_e$  despite large variations in electron density that lead us to infer an approximate factor-of-six variation in the energy input from energetic electrons [Wickwar *et al.*, 1975]. Indeed the elevated electron temperatures occur at a time when the electron density is nearly a minimum. In November the situation is similar. The highest densities, at the two ends and in the middle of the time period, coincide with some of the lowest electron temperatures. The high electron temperatures between 1237 and 1253 and between 1327 and 1332 UT occur in periods of low, though not the lowest, electron densities, while the high temperatures between 1217 and 1222 occur during a period of decreasing electron density. This lack of correlation between electron density and elevated electron temperature is the principal evidence that the elevated temperatures are not due to particle precipitation.

The electron densities, however, do suggest something about the situations under which joule heating occurs. Joule heating is not collocated with auroral arcs (where the densities approach  $10^6 \text{ cm}^{-3}$ ) but rather occurs in regions of reduced ionization, often adjacent to an arc.

#### DISCUSSION AND CONCLUSIONS

Because of the unexpected magnitude of the elevated electron temperatures, we have gone to considerable length in the previous section to establish the reality of the observations

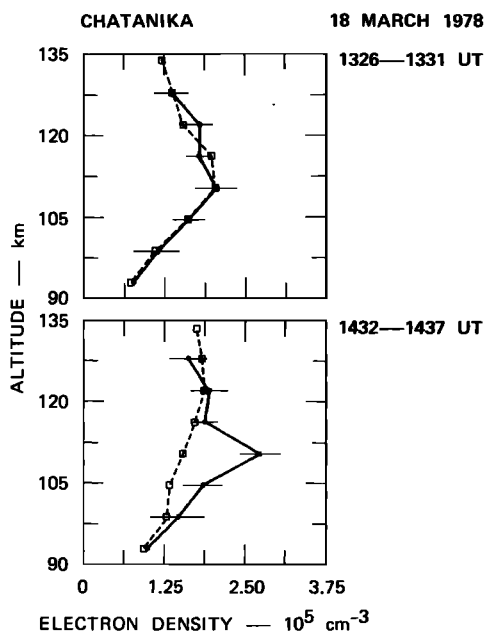


Fig. 7. Raw and corrected electron density profiles for March 18, 1978. The squares connected by dashed lines show the raw density measurements. The circles connected by solid lines show the fully corrected density measurements. (a) Profiles from the typical period, 1326–1331 UT, are indistinguishable. (b) The fully corrected profile from the unusual period, 1432–1437 UT, has its peak density at a significantly lower altitude, and the value is twice as great.

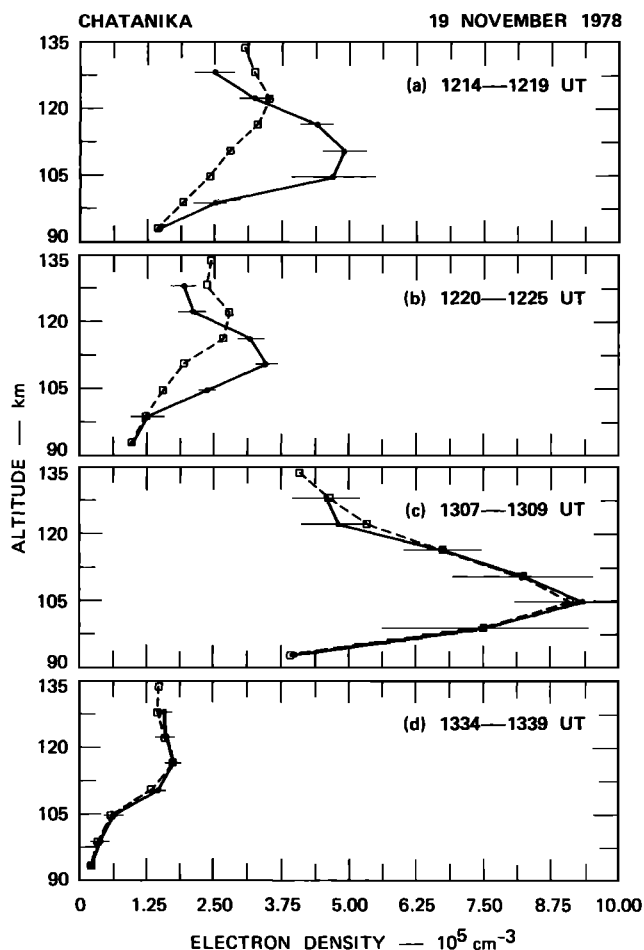


Fig. 8. Raw and corrected electron density profiles for November 19, 1978. The squares connected by dashed lines show the raw density measurements. The circles connected by solid lines show the fully corrected density measurements. For the two later time periods, the two profiles are indistinguishable. For the two earlier time periods, there are large differences. Near 110 km, the much larger densities are due primarily to the elevated electron temperatures. Above 120 km, the lower densities are due primarily to the elevated ion temperatures.

and to establish their interpretation as elevated electron temperatures. Such temperatures may have been seen previously with in situ rocket measurements [Ulwick *et al.*, 1968]. They appear in the data presented by Schlegel *et al.* [1980] and are discussed in a parallel effort to this one by Schlegel and St-Maurice [1981].

Given these temperatures, one of the immediate questions is that of the energy source. From the lack of correlation between the electron densities and the electron temperatures as discussed in the previous section, it is apparent that the energy source is not the incident flux of primary electrons. Instead, the correlation with higher-altitude ion temperatures indicates a relationship with joule heating. Yet the works by Rees and Walker [1968] and Schunk and Walker [1971] show that joule heating of the electrons is negligibly small. Our calculations, which show energy loss rates due to the rotational excitation of  $\text{N}_2$  and  $\text{O}_2$  to be much greater than those due to electron joule heating, confirm these theoretical results for our particular situation. Nonetheless, the electron heating and joule heating are very closely related in that we see the heating when there are 25- to 40-mV/m electric fields or, equivalently, when

the electrons have a velocity relative to the ions and neutrals of 500–800 m/s. These large differential velocities might give rise to an instability [Farley, 1963]. This possibility is being explored by Schlegel and St.-Maurice [1981] and St.-Maurice et al. [1981].

Recently, it has been proposed that there is a plasma instability effective in producing pulsating auroras [Stenbaek-Nielsen and Hallinan, 1979]. It would have to be a different instability than the one required here. In the case of those auroras, the emitting layer was less than 2 km in extent. In our case, as previously discussed, our altitude resolution enables us to be sure that the electron heating extends over an altitude region of at least 15 km. Furthermore, pulsating auroras are not associated with joule heating events.

Another important question to consider is the implication that elevated electron temperatures have for *E* region aeronomy. The electron temperature affects the recombination rates of molecular ions and hence calculations of the energy input or ion production rate due to auroral primary and secondary electrons [Wickwar et al., 1975; Vondrak and Baron, 1976; Oran et al., 1981]. The recombination rates drop by about 25% for an electron temperature increase from 250 to 750 K [Oran et al., 1981].

There is an indirect way in which these temperatures can affect the interpretation of incoherent scatter auroral *E* region data. To date, most *E* region density data determined with the Chatanika radar have assumed that the electron-to-ion temperature ratio was unity. When the temperature ratio is not unity, there can be large corrections that affect both the magnitude of the *E* region peak density and the altitude of the maximum. In Figures 7 and 8, for March 18, 1978, and November 19, 1978, respectively, we show examples of electron density profiles. In Figure 7 at 1325 UT there is good agreement between the raw and the fully corrected densities. Similarly, in Figure 8 at 1308 and 1337 UT there is good agreement. But at 1435 UT in Figure 7 and 1217 and 1222 UT in Figure 8 there is a very great difference between the raw and the fully corrected profiles.

Thus during periods of joule heating there can be significant errors in the derivation of many ionospheric parameters unless the temperatures are measured and the appropriate corrections made. To emphasize this point we give several examples. Since the conductivities are proportional to  $N_e$ , the conductivities near 110 km could double. Because of different conductivity altitude profiles, the ratio of integrated Hall to Pedersen conductivities would increase. Similarly, the deduced currents near 110 km could double. Since the ion production rate is proportional to the electron density squared, the deduced production rate or energy input from energetic particles would increase near 110 km by a factor of 3. (It is not a factor of 4 because the recombination rate is reduced about 25%.) As a consequence, the total energy input would increase substantially, and the deduced spectrum of auroral primary electrons would be shifted considerably toward higher energies.

In conclusion, we have on occasion measured unusual spectra near 110 km that are of ionospheric origin and that can be interpreted only as enhanced electron temperatures. These large temperatures below 116 km cannot be accounted for by either particle precipitation or joule heating; yet they occur simultaneously with large joule heating events. Enhanced electron temperatures will have effects on the *E* region aeronomy, such as causing reduced recombination rates. They

must also be taken into account for the interpretation of the incoherent scatter data during periods of joule heating.

#### APPENDIX: SIGNAL PROCESSING AND THE LEAST SQUARES FIT

In performing the nonlinear least squares fit, we have to allow for the fact that the ACF of the scattering medium  $\rho_{TH}(t)$  is distorted by the pulse sequence and the effective filter pass-band. Ignoring noise and assuming appropriate normalization, the observed ACF is

$$\rho_{OBS}(t) = \int \rho_{TH}(\tau) W(\tau) R_H(t - \tau) d\tau \quad (A1)$$

where  $W(t)$  is the ACF of the transmitted pulse pattern and  $R_H(t)$  is the ACF of the filter impulse response [Farley, 1969; Zamlutti and Farley, 1975; Rino, 1978].

For the low-altitude *E* region measurements,  $\rho_{TH}(t)$  varies slowly compared to  $R_H(t)$ . Therefore  $R_H(t)$  can be considered as a  $\delta$  function compared to  $\rho_{TH}(t)$ , enabling us to approximate (A1) by

$$\rho_{OBS}(t) = \rho_{TH}(t) \int W(\tau) R_H(t - \tau) d\tau \quad (A2)$$

Let us define a complex weighting function

$$S(t) = \int W(\tau) R_H(t - \tau) d\tau \quad (A3)$$

which includes the instrumental effects and can be determined to great precision.

Instead of correcting the theoretical ACF of the scattering medium for  $S(t)$  on each iteration in the least squares fit, we scale the observed ACF by the modulus of  $S(t)$ ,

$$R_{OBS}(t) = \rho_{OBS}(t) / [S(t)S^*(t)]^{1/2} \quad (A4)$$

Since the theoretical ACF is initially calculated with the assumption of no Doppler shift, we do have to correct each term for the ion velocity. At that time, we also correct  $\rho_{TH}(t)$  for the phase,

$$\varphi = \tan^{-1} \left[ \frac{\text{Im } S(t)}{\text{Re } S(t)} \right] \quad (A5)$$

introduced by  $S(t)$ . Thus, ignoring the ion velocity, we create

$$R_{TH}(t) = \rho_{TH}(t) e^{i\varphi} \quad (A6)$$

In the least squares fitting procedure we then vary the fitting parameters determining  $\rho_{TH}(t)$ , hence  $R_{TH}(t)$ , so as to obtain the best match between  $R_{OBS}(t)$  and  $R_{TH}(t)$ . The fit minimizes the reduced chi square,

$$\chi_R^2 = \sum_{i=0}^{31} \left\{ \frac{[R_{OBS}(i) - R_{TH}(i)]^2}{\sigma^2(i) / [S(i)S^*(i)]} \right\} / (32 - N) \quad (A7)$$

where  $N$  is the number of parameters being fitted and  $\sigma^2(i)$  is the estimate of the variance of  $\rho_{OBS}$ , which will be given below. Because of the direct IF sampling, only the real parts of  $R_{OBS}$  and  $R_{TH}$  will be compared for  $i$  even and only the imaginary parts for  $i$  odd. So long as  $\chi_R^2$  is reduced by each iteration, the iterations continue until the calculated increment for every fitting parameter is less than 25% of the uncertainty of that parameter. A maximum of six good iterations is performed.

The variance for each lag  $\sigma^2(i)$  is estimated from the real part of the observed ACF. The real part is interpolated to obtain its value at the time when only the imaginary component is observed. The variance is given by

$$\sigma^2(0) = \frac{2}{N_{\text{pulse}}} \left\{ 1 + \frac{2}{\text{SNR}} + \frac{2}{(\text{SNR})^2} \right\} \quad (\text{A8a})$$

for the zero lag,

$$\sigma^2(i) = \frac{1}{N_{\text{pulse}}} \left\{ \rho_{\text{OBS}}^2(i) + 1 + \frac{2}{\text{SNR}} + \frac{2}{(\text{SNR})^2} \right\} \quad (\text{A8b})$$

for the other unipulse lags ( $1 \leq i \leq 5$ ), and

$$\sigma^2(i) = \frac{1}{N_{\text{pulse}}} \left\{ \rho_{\text{OBS}}^2(i) + 9 + \frac{6}{\text{SNR}} + \frac{2}{(\text{SNR})^2} \right\} \quad (\text{A8c})$$

for the remaining lags, where  $N_{\text{pulse}}$  is the number of transmitted pulses and SNR is the signal-to-noise ratio.

As we go above about 120 km under 'normal' E region conditions or when we have the elevated electron temperatures, we can no longer assume that  $\rho_{\text{TH}}(t)$  varies more slowly than  $R_H(t)$ . The approximation enabling us to obtain (A2), then, breaks down. Instead, we use the Fourier transform of (A1):

$$s_{\text{OBS}}(f) = H(f) \int w(f-f') s_{\text{TH}}(f') df' \quad (\text{A9})$$

where  $H(f)$  is the filter spectrum and  $w(f)$  is the spectrum of the transmitted pulse. We now inverse-filter the observed spectrum,

$$s'(f) = s_{\text{OBS}}(f)/H(f) \quad (\text{A10})$$

and Fourier transform back to the time domain,

$$\rho'(t) = W(t)\rho_{\text{TH}}(t) \quad (\text{A11})$$

For the least squares fit we define

$$R_{\text{OBS}}(t) = \rho'(t)/W(t) \quad (\text{A12})$$

Ignoring ion velocity, it is this  $R_{\text{OBS}}$  that is compared to the theoretical ACF in the least squares fitting procedure as previously described.

This simpler procedure, based on (A9), is not applicable at the lower altitudes because the longer correlation time of the medium leads to nonzero values for the last lags. In the transition zone above 120 km, where we pass from the applicability of the method involving the complex weighting function to the method involving inverse filtering, the difference between the answers is not great. The electron and ion temperatures near 110 km are about 10% greater with the complex weighting function method. The electron density is virtually unchanged. All the data presented here were found using the complex weighting function method. However, for the large electron temperatures, the correlation time is decreased enough that the inverse filtering method would be more appropriate. At most, the electron temperatures are overestimated due to this effect by about 5%.

*Acknowledgments.* We would like to thank the staff members at SRI International and CEPHAG who made these joint experiments and collaboration possible. In particular, we would like to thank J. Kelly, M. McCready, C. Code, and C. D. Feken for their assistance at Chatanika and C. Dawson and C. Leger for programming. The French portion of the experiment was supported by the Actions Thematiques Programmees of the Centre National de la Recherche

Scientifique for the International Magnetospheric Study. It was supported, as well, by the Centre de Recherches en Physique de l'Environnement Terrestre et Planetaire and by the Centre National d'Etudes des Telecommunications. The American portion was supported by grants ATM78-00129 and ATM78-23658 from the Aeronomy Program, Division of Atmospheric Sciences, National Science Foundation. In addition, the Chatanika radar was operated by SRI International under contract DNA001-77-C-0042 from the Defense Nuclear Agency and grant ATM72-01644-A05 from the Division of Atmospheric Sciences, National Science Foundation.

The Editor thanks J. V. Evans and E. Fonthelm for their assistance in evaluating this paper.

## REFERENCES

- Bevington, P. R., *Data Reduction and Error Analysis for the Physical Sciences*, McGraw-Hill, New York, 1969.
- de la Beaujardiere, O., V. B. Wickwar, C. A. Leger, M. McCready, and M. J. Baron, The software system for the Chatanika incoherent scatter radar, technical report, 117 pp., SRI Int., Menlo Park, Calif., 1980.
- de la Beaujardiere, O., R. R. Vondrak, R. A. Heelis, W. B. Hanson, and R. Hoffman, Auroral arc electrodynamic parameters measured by AE-C and the Chatanika radar, *J. Geophys. Res.*, **86**, in press, 1981.
- Evans, J. V., Theory and practice of ionosphere study by Thomson scatter radar, *Proc. IEEE*, **57**, 469-530, 1969.
- Farley, D. T., A plasma instability resulting in field-aligned irregularities in the ionosphere, *J. Geophys. Res.*, **68**, 6083-6097, 1963.
- Farley, D. T., Incoherent scatter correlation function measurements, *Radio Sci.*, **4**, 935-953, 1969.
- Hagfors, T., Least mean square fitting of data to physical models, *EISCAT Tech. Note 78/2*, Kiruna, Sweden, 1978.
- Jacchia, L. G., Revised static models of the thermosphere and exosphere with empirical temperature profiles, *Spec. Rep. 332*, Smithsonian Astrophys. Observ., Cambridge, Mass., 1971.
- Kelly, J. D., and V. B. Wickwar, Radar measurements of high-latitude ion composition between 140 and 300 km, submitted to *J. Geophys. Res.*, 1981.
- Kofman, W., and V. B. Wickwar, Plasma line measurements at Chatanika with high-speed correlator and filter bank, *J. Geophys. Res.*, **85**, 2998-3012, 1980.
- Leadbrand, R. L., M. J. Baron, J. Petriceks, and H. F. Bates, Chatanika, Alaska, auroral-zone incoherent-scatter facility, *Radio Sci.*, **7**, 747-756, 1972.
- Lejeune, G., EISCAT data analysis, *Rep. 36/78*, Centre d'Etude des Phenomenes Aleatoires et Geophys., St. Martin d'Heres, France, 1978.
- Lejeune, G., A program library for incoherent scatter calculation, *EISCAT Tech. Note 79/18*, Kiruna, Sweden, 1979.
- Oran, E. S., V. B. Wickwar, W. Kofman, and A. Newman, Auroral plasma lines: A first comparison of theory and experiment, *J. Geophys. Res.*, **86**, 199-205, 1981.
- Rees, M. H., and J. C. G. Walker, Ion and electron heating by auroral electric fields, *Ann. Geophys.*, **24**, 193-199, 1968.
- Rees, M. H., R. A. Jones, and J. C. G. Walker, The influence of field-aligned currents on auroral electron temperatures, *Planet. Space Sci.*, **19**, 313-325, 1971.
- Rino, C. L., Incoherent scatter radar signal processing techniques, technical memo, SRI Int., Menlo Park, Calif., 1978.
- Rino, C. L., M. J. Baron, G. H. Burch, and O. de la Beaujardiere, A multipulse correlator design for incoherent scatter radar, *Radio Sci.*, **9**, 1117-1127, 1974.
- Schlegel, K., and J. P. St.-Maurice, Anomalous heating of the polar E region by unstable plasma waves, I, Observations, *J. Geophys. Res.*, **86**, 1447-1452, 1981.
- Schlegel, K., H. Kohl, and K. Rinnert, Temperatures and collision frequency in the polar E region measured with the incoherent scatter technique, *J. Geophys. Res.*, **85**, 710-714, 1980.
- Schunk, R. W., Transport equations for aeronomy, *Planet. Space Sci.*, **23**, 437-485, 1975.
- Schunk, R. W., and J. C. G. Walker, Transport processes in the E region of the ionosphere, *J. Geophys. Res.*, **76**, 6159-6171, 1971.
- Schunk, R. W., and J. C. G. Walker, Theoretical ion densities in the lower atmosphere, *Planet. Space Sci.*, **21**, 1875-1896, 1973.
- Stenbaek-Nielsen, H. C., and T. J. Hallinan, Pulsating auroras: Evi-

- dence for noncollisional thermalization of precipitating electrons, *J. Geophys. Res.*, **84**, 3257–3271, 1979.
- St.-Maurice, J. P., and K. Schlegel, Anomalous heating of the polar *E* region by unstable plasma waves, II, Theory, *J. Geophys. Res.*, **86**, 1453–1462, 1981.
- Ulwick, J. C., W. Pfister, and K. D. Baker, Rocket measurements of Bremsstrahlung x-rays and related parameters during auroral absorption events, *Space Res.*, **8**, 171–177, 1968.
- Vondrak, R. R., and M. J. Baron, Radar measurements of the latitudinal variations of auroral ionization, *Radio Sci.*, **11**, 939–946, 1976.
- Walker, J. C. G., and M. H. Rees, Ionospheric electron densities and temperatures in aurora, *Planet. Space Sci.*, **16**, 459–475, 1968.
- Wickwar, V. B., Chatanika radar measurements, in *Atmospheres of Earth and the Planets*, pp. 111–124, D. Reidel, Hingham, Mass., 1975.
- Wickwar, V. B., M. J. Baron, and R. D. Sears, Auroral energy input from energetic electrons and joule heating at Chatanika, *J. Geophys. Res.*, **80**, 4364–4367, 1975.
- Zamlutti, C. J., and D. T. Farley, Incoherent scatter multiple-pulse measurements at Arecibo, *Radio Sci.*, **10**, 573–580, 1975.

(Received July 1, 1980;  
revised December 16, 1980;  
accepted December 17, 1980.)